BAMS Article

How Does Boundary Layer Meteorology–Photochemistry Coupling Govern Winter $PM_{2.5}$ Pollution? Insights from Intensive Vertical Observations in a River Valley Basin

Pengfei Tian,[a] Min Zhang,[a,c] Xiaoxue Liu,[a] Jiayun Li,[a] Zeren Yu,[a] Xin Song,[a] Xu Guan,[a] Chenguang Tang,[d] Yan Ren,[b] Jiening Liang,[a] Xianjie Cao,[a] Lei Zhang,[a,b] and Jianping Huang[a,b]

KEYWORDS:
Atmosphere;
Boundary layer;
Aerosols;
Air quality

ABSTRACT: Basin cities worldwide continue to experience severe winter particulate pollution despite global air pollution control efforts, highlighting unresolved atmospheric boundary layer (ABL) meteorology–chemistry coupling. To address this issue, we conducted an intensive field campaign in the river valley basin of Lanzhou in northwestern China during January 2021, complemented by 3-yr continuous monitoring at a superstation. We categorized particulate pollution into three levels based on particulate matter that is smaller than 2.5 μm in diameter ($PM_{2.5}$) concentrations: excellent (32.8 μg m^{-3}), good (60.0 μg m^{-3}), and polluted (83.3 μg m^{-3}). Results show that, despite comparable aerosol optical depth, surface $PM_{2.5}$ under the polluted level was markedly higher (23.3 μg m^{-3}) than under the good level, owing to contrasting aerosol vertical distributions. The ABL meteorology played a dominant role in aerosol vertical distribution through controlling vertical exchange processes, with basinwide instability [gradient Richardson number (Ri) < 0.25] under the excellent level, lower-basin instability (Ri < 0.25) and upper-basin stability (Ri > 0.25) under the good level, and basinwide strong stability under the polluted level. Most notably, we observed the largest day–night aerosol extinction coefficients difference of 0.07 km^{-1} at ~0.42-km altitude under the good level, demonstrating peak photochemical conversion of secondary inorganic aerosols in the upper ABL. This phenomenon is driven by the boundary layer meteorology that efficiently transports surface-emitted precursors upward but still confines them within the basin. These findings advance our mechanistic understanding of ABL meteorology–chemistry coupling, establish physical constraints for improving air quality forecasting, and enable optimized pollution control strategies in basin cities worldwide.

DOI: 10.1175/BAMS-D-25-0277.1
Corresponding authors: P. Tian, tianpf@lzu.edu.cn; J. Huang, hjp@lzu.edu.cn
Pengfei Tian and Min Zhang these authors contributed equally to this study.
Supplemental information related to this paper is available at the Journals Online website: https://doi.org/10.1175/BAMS-D-25-0277.s1.

Manuscript received 22 January 2026, in final form 1 June 2026, accepted 17 July 2026

© 2026 American Meteorological Society. This published article is licensed under the terms of the default AMS reuse license. For information regarding reuse of this content and general copyright information, consult the AMS Copyright Policy (www.ametsoc.org/PUBSReuseLicenses).

Brought to you by Lanzhou University | Unauthenticated | Downloaded 11/10/26 10:07 AM UTC

SIGNIFICANCE STATEMENT: Aerosol vertical distribution in the atmospheric boundary layer (ABL) critically modulates surface particulate matter that is smaller than 2.5 μm in diameter ($PM_{2.5}$) pollution, especially in topographically constrained basins. This study demonstrates that even under similar columnar aerosol loading, surface $PM_{2.5}$ concentrations can differ significantly due to distinct aerosol vertical distributions driven by ABL meteorology–photochemistry coupling. For the first time in a semiarid river valley basin, we observe a peak in day–night aerosol loading difference at ~0.42-km altitude under moderate pollution, indicative of enhanced photochemical conversion of secondary inorganic aerosols. These results establish a mechanistic basis for reconciling surface and column aerosol measurements and provide physical constraints for improving air quality forecasting and targeted pollution control in basin cities globally.

AFFILIATIONS: [a] Key Laboratory for Semi-Arid Climate Change of the Ministry of Education, College of Atmospheric Sciences, Lanzhou University, Lanzhou, China; [b] Collaborative Innovation Center for Western Ecological Safety, Lanzhou University, Lanzhou, China; [c] Donghai Laboratory, Zhoushan, China; [d] Guangzhou Institute of Tropical and Marine Meteorology, China Meteorological Administration, Guangzhou, China

1. Introduction

Ambient air pollution poses significant threats to human health and ecological systems, prompting widespread global mitigation efforts in recent decades (Lelieveld et al. 2015; He et al. 2021; Ghude et al. 2024). Substantial progress has been made in air pollution control worldwide, with particularly significant advancements achieved during recent years such as in China (Ouyang et al. 2022; Zhang et al. 2019; Geng et al. 2024). However, wintertime particulate pollution remains a persistent global challenge, despite substantial reductions in primary emissions (Zheng et al. 2015; Thomas et al. 2019; Leung et al. 2020). This issue is particularly acute in basin cities, where pollution episodes lead to significant excess mortality and severe ecological consequences (Finardi et al. 2014; Gu et al. 2023; Yang et al. 2025). Given the unique meteorological and topographic conditions that exacerbate pollution accumulation in basins, targeted research on the formation mechanisms of basin city pollution is urgently needed to develop effective mitigation strategies.

The atmospheric boundary layer (ABL) plays a pivotal role in air pollution through its thermal and dynamic processes that govern ABL structure and regulate vertical air mass exchange (Baklanov et al. 2011; Miao et al. 2019; Shi and Hu 2020; Canché-Cab et al. 2024). A key feature of ABL influence is the capping inversion layer, which traps surface-emitted pollutants, making boundary layer height (BLH) a pivotal determinant of pollution dispersion (Guo et al. 2020; Li et al. 2021; Prasad et al. 2022). Although an inverse BLH–particulate matter that is smaller than 2.5 μm in diameter ($PM_{2.5}$) relationship has been widely studied, observational evidence reveals complex aerosol vertical distributions that can decouple this linkage (Tian et al. 2017; Su et al. 2020; Ratnam et al. 2021; Sun et al. 2021; Huang et al. 2023). Furthermore, the aerosol vertical distribution patterns are particularly important for interpreting the relationships between columnar aerosol loading [aerosol optical depth (AOD)] and surface $PM_{2.5}$ (van Donkelaar et al. 2006; Li et al. 2016; Xin et al. 2016; Prabhakar et al. 2017). In particular, seasonal AOD maxima in summer contrast with winter $PM_{2.5}$ peaks over Europe and the North China Plain, highlighting how aerosol stratification can drive

Brought to you by Lanzhou University | Unauthenticated | Downloaded 11/10/26 10:07 AM UTC

divergent trends in columnar versus ground-level measurements (Koelemeijer et al. 2006; Ma and Yu 2014; Qu et al. 2016; Zhao et al. 2018; Di Antonio et al. 2023). Despite advances in modeling, significant uncertainties persist in simulating pollution processes, particularly in capturing aerosol vertical distributions due to incomplete representations of ABL physics (Kipling et al. 2016; Watson-Parris et al. 2019; Jia and Zhang 2020; Yorks et al. 2023). These challenges are exacerbated in topographically complex regions such as basin cities, where terrain-induced ABL modifications further complicate pollution accumulation mechanisms (Whiteman et al. 2014; Pace et al. 2015; Zhang et al. 2024; Zhao et al. 2023). Thus, elucidating the interplay among ABL processes, surface pollutant concentrations, and columnar aerosol loading remains an urgent priority—especially in basin environments where unique topography and meteorology amplify ABL effects on pollution accumulation.

Chemical processes also play a key role in ABL particulate pollution. Ground-based observations have demonstrated that photochemical conversion and heterogeneous/aqueous-phase reaction processes are major sources of secondary aerosols (Huang et al. 2014; Zhang et al. 2015; George et al. 2015). Vertical profiling studies utilizing multiple platforms (e.g., meteorological towers and unmanned aerial vehicles) have further identified distinct new particle formation mechanisms and secondary aerosol generation processes at different altitudes (Platis et al. 2016; Lei et al. 2021; Li et al. 2022; H. Wang et al. 2025). Advances in ABL meteorology and chemical process research, along with enhanced observational capabilities, have highlighted the importance of their interactions in urban air pollution formation (Xin et al. 2015; Baasandorj et al. 2017; Hao et al. 2018; Zhou et al. 2020; Ma et al. 2020; Lampilahti et al. 2021; Xin et al. 2023; Y. Wang et al. 2025). Numerical modeling studies indicate that enhanced secondary aerosol production in the upper ABL and residual layer significantly exacerbates surface particulate pollution through vertical mixing processes (Huang et al. 2020). However, our understanding of the coupled effects of ABL meteorology and chemistry on aerosol vertical distribution and surface pollution remains incomplete, primarily due to limited comprehensive ABL observations (Li et al. 2017; Wang et al. 2022; Zhu et al. 2023). A recent field campaign in western U.S. basins has begun to address this knowledge gap by investigating air quality–boundary layer interactions (Hallar et al. 2021; Carrillo-Cardenas et al. 2025). Given the global prevalence of severe winter $PM_{2.5}$ pollution in basin cities, there is an urgent need for expanded observational studies across different climatic regions to better elucidate these complex interactions.

The Lanzhou basin, located in the semiarid region of northwest China, is another prominent example of severe winter $PM_{2.5}$ pollution (T. Du et al. 2020; Zhang et al. 2024). To investigate the coupled effects of ABL meteorology and photochemistry on wintertime $PM_{2.5}$ formation mechanisms in this unique basin environment, we conducted an intensive field campaign. This study combines 3 years of routine observations from a superstation with intensive vertical profiling of meteorological parameters, aerosol extinction coefficients, and chemical composition. These measurements provide critical observational evidence for understanding how ABL–photochemistry interactions drive particulate pollution. As global air quality management faces persistent challenges despite significant progress in emission control, this research offers valuable insights for developing targeted pollution mitigation strategies in basin cities, particularly in arid and semiarid regions worldwide.

2. Field campaigns and data

a. Design of the field campaigns. Lanzhou, a representative river valley basin city situated in the semiarid region of northwestern China, is geographically constrained by mountain ranges to both its northern and southern peripheries (Fig. 1). To investigate air pollution mechanisms in this topographically complex and semiarid urban environment, the Lanzhou Atmospheric Components Monitoring Superstation (LACMS; 36.05°N, 103.87°E, 1520 m MSL)

Brought to you by Lanzhou University | Unauthenticated | Downloaded 11/10/26 10:07 AM UTC

was established to systematically measure physical and chemical properties of gaseous and particulate pollutants. This study combines routine measurements from the LACMS station with vertical observations from an intensive field campaign to better elucidate particulate pollution mechanisms, particularly the coupled impact of atmospheric boundary layer meteorology and photochemistry on winter basin city $PM_{2.5}$ pollution.

This study utilizes particulate matter (PM) concentrations, aerosol optical properties, chemical compositions, gas concentrations, and meteorological parameters at the LACMS station from 2020 to 2022. The intensive field campaign in January 2021 collected vertical profiles of meteorological parameters and aerosol extinction coefficients, as well as $PM_{2.5}$ chemical components at both the surface and an elevated station situated at the southern slope crest of the basin (referred to as the "basin top," approximately 630 m above the basin floor). This intensive field campaign enabled vertical characterization of pollutants and meteorology under the basin's unique topography. Detailed instrument information is provided in Table S1 in the online supplemental material.

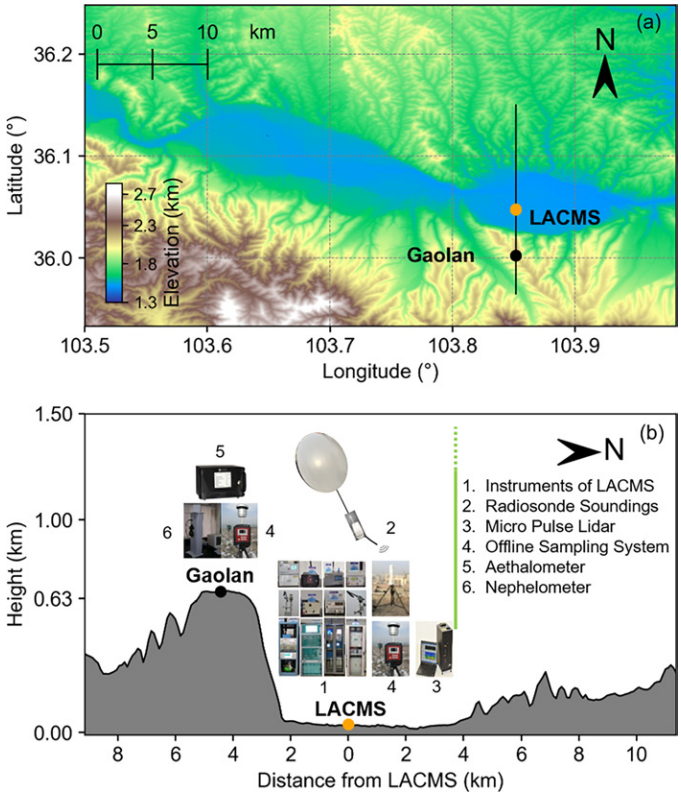


FIG. 1. Schematic of the (a) basin topography and (b) field campaign design. The gray shading in (b) depicts the terrain elevation along the longitudinal section across the LACMS station. The LACMS station (orange dot) is located at the basin floor, while the elevated monitoring site (black dot) is positioned at the basin top.

b. Measurements at the LACMS station. The LACMS is located in the densely populated urban center of the Lanzhou basin and has been operational since 2019. Routine measurements at the station include PM concentrations of different sizes (PM_1, $PM_{2.5}$, PM_{10}, and TSP), aerosol optical properties (scattering and absorption from ultraviolet to infrared wavelengths), chemical compositions (water-soluble inorganic ions, carbonaceous components, and metallic elements), aerosol vertical distribution (extinction coefficients at 532 nm), gas concentrations [sulfur dioxide (SO_2), nitrogen dioxide (NO_2), carbon monoxide (CO)], and meteorological parameters [temperature (T), relative humidity (RH), air pressure (P), wind direction (WD), wind speed (WS), and turbulent kinetic energy (TKE)] (Table S1). The station is operated and maintained by dedicated personnel, and the data undergo rigorous quality control. Calculation of sulfur oxidation ratio (SOR), nitrogen oxidation ratio (NOR), primary organic carbon (POC), and secondary organic carbon (SOC) is introduced in the supplemental (Text 1). Part of the data has been applied in scientific research and local pollution control efforts (T. Du et al. 2020; Guan et al. 2021; Chang et al. 2022).

To analyze the characteristics and processes of varying fine particulate pollution levels, observations from winter 2020 to 2022 were categorized into excellent (daily $PM_{2.5} \leq 35\ \mu g\ m^{-3}$), good ($35 <$ daily $PM_{2.5} < 75\ \mu g\ m^{-3}$), and polluted (daily $PM_{2.5} \geq 75\ \mu g\ m^{-3}$) pollution

Brought to you by Lanzhou University | Unauthenticated | Downloaded 11/10/26 10:07 AM UTC

levels. The proportions of days with excellent, good, and polluted levels were 17% (46 days), 54% (147 days), and 29% (78 days), respectively.

c. Vertical observations during the intensive field campaign. To compensate for the LACMS station's limitations in vertical observations, the intensive field campaign collected profiles of aerosols and meteorological parameters, as well as chemical components at both the basin floor and top. The campaign was conducted from 4 to 31 January 2021 [Beijing time (BJT); BJT = UTC + 8]. Excluding three snowy days, the proportions of the excellent, good, and polluted days were 20% (5 days), 56% (14 days), and 24% (6 days), respectively.

The $PM_{2.5}$ offline samples were simultaneously collected at the basin floor (60 samples) and top (59 samples). These samples were analyzed for chemical components, including water-soluble inorganic ions, carbonaceous components, and metallic elements. Organic carbon (OC) was further divided into POC and SOC using the minimum OC/elemental carbon (EC) ratio method (Cao et al. 2007). Instrument and method details for the $PM_{2.5}$ offline sampling are described in the supplemental (Text 2).

A mobile micropulse lidar (MPL) was used to measure the continuous vertical distribution of aerosols at 532 nm with a blind zone of 100 m, a vertical resolution of 30 m, and a temporal resolution of 1 min. Hourly aerosol extinction coefficient profiles were derived from lidar data using the Fernald method and simulated annealing algorithm (Fernald 1984; M. Zhang et al. 2021). The detailed method is described in the supplemental (Text 3). A total of 511 aerosol extinction coefficient profiles were obtained, including 43, 337, and 131 profiles for the excellent, good, and polluted levels, respectively. The AOD below 2.5 km was calculated by integrating the extinction coefficient from the surface to 2.5 km. The lidar-derived AOD exhibited good correlation with the sun photometer–derived AOD (Fig. S1).

A total of 66 radiosondes were launched at the LACMS station at 0200, 0800, 1100, 1400, 1700, and 2000 BJT, yielding high-resolution (5–7 m) profiles of *T*, *P*, RH, WS, and WD. The BLH and residual layer height were derived from radiosonde soundings by the Liu and Liang method (Liu and Liang 2010), which showed excellent correlation with lidar data (Fig. S1). The Froude number (Fr), a function of wind speed and atmospheric stability, can reflect the horizontal diffusion intensity:

$$\mathrm{Fr} = U_0 \left(gH \frac{\Delta\theta}{\overline{\theta}} \right)^{-1/2}, \tag{1}$$

where U_0 is the wind speed at 10 m, g is the gravitational acceleration (9.8 m s^{-2}), H is the height of the obstacle (630 m in this study), $\Delta\theta$ is the increase in potential temperature between the surface and the top of the basin [Fr is meaningful (real) if the temperature increases with height], and $\overline{\theta}$ is the average potential temperature of the layer between the surface and the top height of the basin. The gradient Richardson number (Ri) is defined as

$$\mathrm{Ri} = \frac{\dfrac{g}{\overline{\theta}} \dfrac{\Delta\overline{\theta}}{\Delta z}}{\left(\dfrac{\Delta u}{\Delta z} \right)^2 + \left(\dfrac{\Delta v}{\Delta z} \right)^2} = \frac{N^2}{S^2}, \tag{2}$$

where Δz is the height increment for calculating Ri; g is the gravitational acceleration; $\overline{\theta}$ is the average virtual potential temperature; and $\Delta\overline{\theta}/\Delta z$, $\Delta u/\Delta z$, and $\Delta v/\Delta z$ are the vertical gradients of the potential temperature, east–west wind, and north–south wind components, respectively. The N is the Brunt–Väisälä frequency and S is the total vertical shear. The Ri data were categorized into three regimes (Balsley et al. 2008): unstable regime, Ri < 0.25, where turbulent energy is dominated by kinetic energy; transition regime, 0.25 < Ri < 1, characterized

Brought to you by Lanzhou University | Unauthenticated | Downloaded 11/10/26 10:07 AM UTC

by rapidly decreasing normalized fluxes with increasing stability; and very stable regime, Ri > 1, characterized by small but finite momentum flux. The Ri can vary by two or more orders of magnitude due to changes in buoyancy and wind shear (e.g., Luce et al. 2018; Yang et al. 2023). Accordingly, following previous studies, the median is used to characterize its vertical distribution. The median Ri along with the interquartile range (25th–75th percentiles) for the excellent, good, and polluted levels is shown in Fig. S2.

3. Impacts of boundary layer meteorology on aerosol vertical distribution and particulate pollution level

a. Relationships between surface $PM_{2.5}$ and aerosol vertical distributions under different particulate pollution levels. The $PM_{2.5}$ pollution in Lanzhou basin remains high despite strict national and local government controls in China. Observations from the LACMS station reveal wintertime $PM_{2.5}$ concentrations averaging 54.6 ± 27.0 (average ± standard deviation), 62.8 ± 33.1, and 72.1 ± 32.8 $\mu g\ m^{-3}$ in the winters of 2020, 2021, and 2022, respectively—far exceeding the World Health Organization recommended annual guideline of 5 $\mu g\ m^{-3}$ (World Health Organization 2021). Furthermore, under different pollution levels, mean $PM_{2.5}$ concentrations reached 26.5 ± 6.0 $\mu g\ m^{-3}$ (excellent), 56.0 ± 11.6 $\mu g\ m^{-3}$ (good), and 92.3 ± 12.5 $\mu g\ m^{-3}$ (polluted), highlighting persistent exposure risks especially under the polluted level. Such severe particulate pollution poses significant public health threats, underscoring the urgent need to elucidate its underlying mechanisms for effective mitigation. While anthropogenic emissions are a key contributor, we hypothesize that the interplay of boundary layer meteorology, photochemical processes, and their synergistic effects play a critical role in sustaining high $PM_{2.5}$ pollution in this northwestern Chinese basin. This study aims to address these scientific gaps using intensive vertical observations in Lanzhou basin.

Lidar observations further demonstrate that PM concentrations in the boundary layer are the highest under the polluted level and the lowest under the excellent level (Fig. 2). These pollutants were predominantly confined to the basin, with the worst pollution between 0900 and 1200 BJT. PM progressively accumulated near the basin floor after sunrise and rapidly diffused after approximately 1200 BJT when the BLH surpassed the basin top. The daytime boundary layer developed the highest (with a maximum BLH of 1560 m) under the excellent level, while it developed the lowest (with a maximum BLH of 868 m) under the polluted level. This particulate pollution diurnal pattern in the Lanzhou basin contrasts markedly with that observed in other urban areas, such as Beijing (Li et al. 2022) and Shanghai (Zhang et al. 2025), where PM typically peaks during nighttime due to variations in atmospheric dispersion conditions.

To elucidate the mechanisms governing the relationship between aerosol vertical distributions and surface $PM_{2.5}$ pollution, an intensive observational campaign was conducted in January 2021, capturing simultaneous vertical profiles of meteorological parameters and particulate pollutants. Surface $PM_{2.5}$ concentrations exhibited a pronounced increase with deteriorating air quality, averaging 32.8 ± 16.0, 60.0 ± 19.8, and 83.3 ± 18.8 $\mu g\ m^{-3}$ under the excellent, good, and polluted levels, respectively (Fig. 3a and Fig. S3; Table S2). The columnar AOD remained low under the excellent level. However, AOD values under the good (0.27 ± 0.14) and polluted (0.26 ± 0.11) levels were comparable, despite the significantly differing $PM_{2.5}$ concentrations. Consistent with the surface $PM_{2.5}$ trend, near-surface aerosol extinction coefficients increased markedly with pollution severity, averaging 0.15, 0.30, and 0.47 km^{-1} for the excellent, good, and polluted levels, respectively. However, the aerosol vertical distributions diverged substantially across pollution levels (Fig. 3b), suggesting possible reasons for the inconsistency between surface $PM_{2.5}$ and columnar AOD trends. Data during the winter months (January, February, and December) from 2020 to 2022 yielded similar results: $PM_{2.5}$ rapidly increased with

Brought to you by Lanzhou University | Unauthenticated | Downloaded 11/10/26 10:07 AM UTC

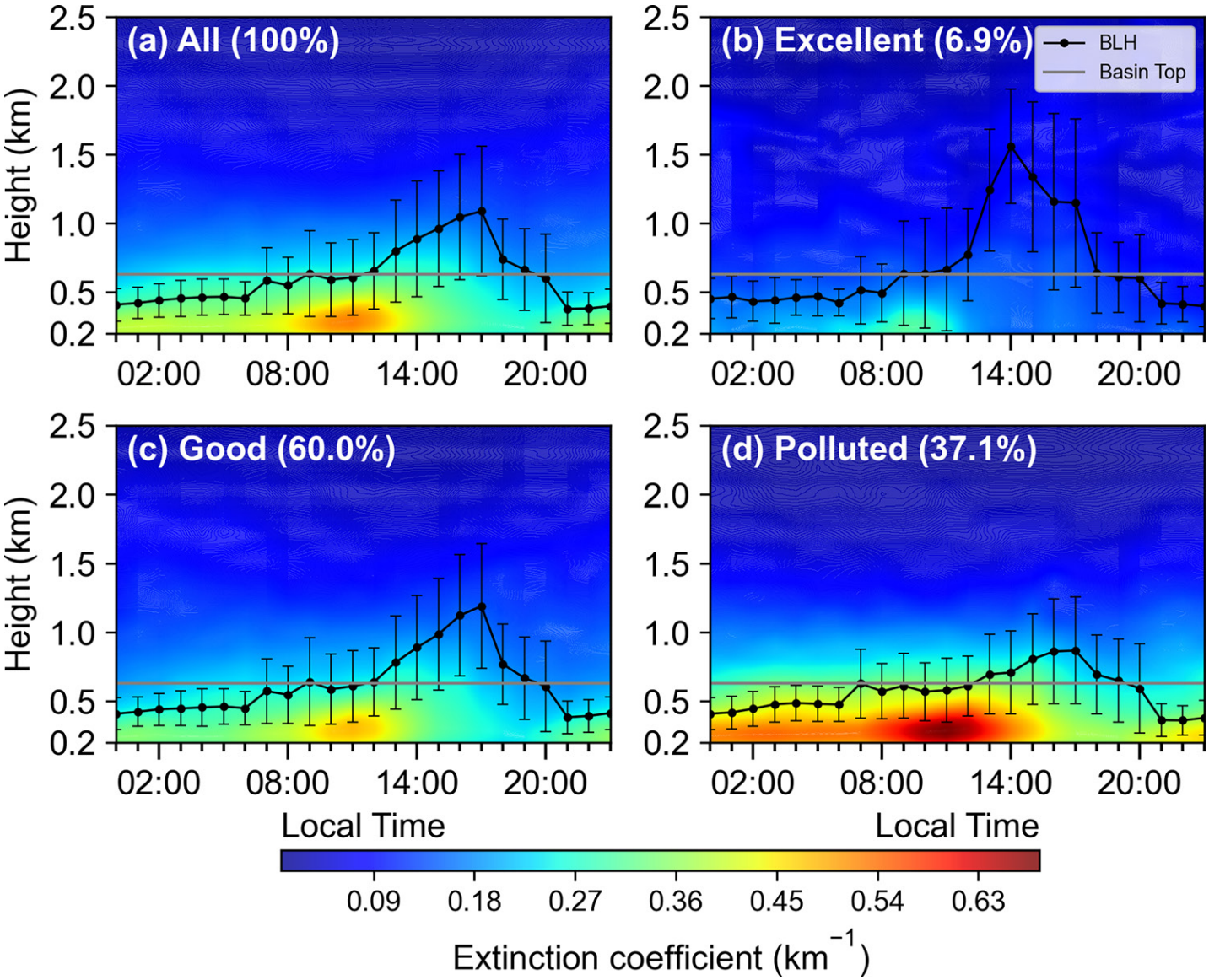


FIG. 2. Wintertime aerosol vertical distribution from lidar observations (2020–22) categorized by $PM_{2.5}$ pollution levels: (a) total observations and (b) under the excellent, (c) good, and (d) polluted levels. The dotted black and the gray lines represent BLH and the basin top, respectively. BLH uncertainty (±1 standard deviation) reflects both instrumental and retrieval variability across the observational dataset.

increasing pollution severity, while there was little difference between AOD values under the good and polluted levels (Fig. S4).

The vertical distribution of aerosols (Fig. S5) was quantified using the extinction lapse-rate parameter (Tian et al. 2017), which exhibited values of 0.06, 0.12, and 0.19 km^{-2} under the excellent, good, and polluted levels, respectively. Under the excellent level, both the extinction coefficients and the extinction lapse rate remained relatively low throughout the atmospheric column. The higher extinction coefficient near the surface and the faster decay (higher extinction lapse rate) in the vertical direction, under the polluted level than under the good one, led to an intersection of the extinction profiles at ~0.63-km altitude. This vertical structure explains the comparable columnar AOD values observed under the good and polluted levels, despite their markedly different surface aerosol loadings. This phenomenon contrasts with observations from other regions (e.g., Y. Zhang et al. 2021), where columnar AOD rapidly increases with worsening pollution levels. The underlying drivers of these distinct aerosol vertical distributions, particularly the role of boundary layer meteorology, are investigated in the following section.

Brought to you by Lanzhou University | Unauthenticated | Downloaded 11/10/26 10:07 AM UTC

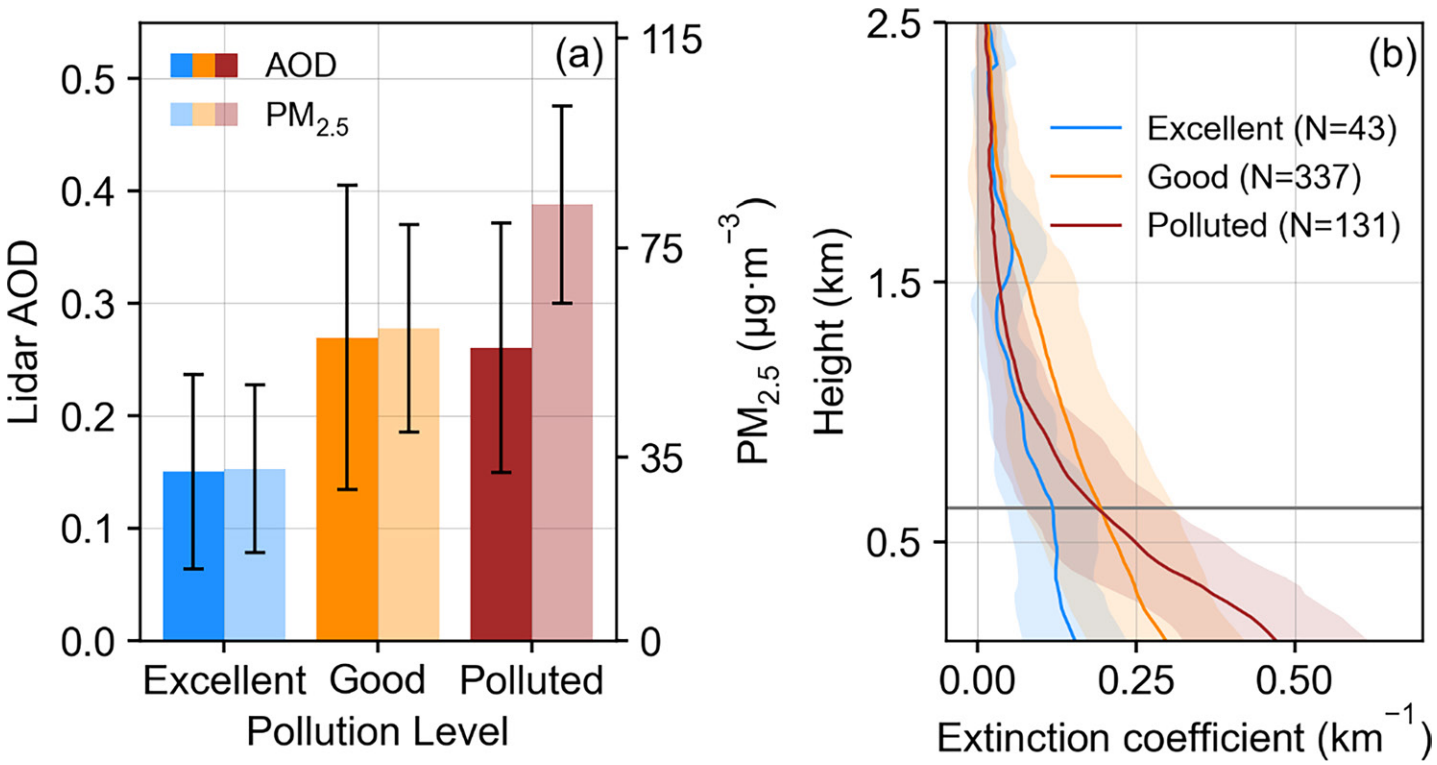


FIG. 3. Surface $PM_{2.5}$, columnar AOD, and vertical distribution of aerosols under different pollution levels in January 2021: (a) $PM_{2.5}$ at the surface and columnar AOD below 2.5 km and (b) vertical distribution of aerosol extinction coefficients (±1 standard deviation). The gray horizontal line indicates the basin-top height.

b. Boundary layer meteorology affects aerosol vertical distribution under different particulate pollution levels. To elucidate the boundary layer meteorological processes governing particulate pollution in the Lanzhou basin, considering the terrain, local-scale meteorology, and aerosol transport, high-resolution WRF with Chemistry (WRF-Chem) numerical simulations were conducted using a two-way nested model. The model setup adopted horizontal resolutions of 2 and 10 km for the nested domains, respectively, and enhanced vertical resolution of 40 layers up to 50 hPa as documented by Wang et al. (2019). The simulated wind speed and potential temperature profiles show a reasonable agreement with the observations (Fig. S6). The air temperature increased with increasing pollution severity (Fig. 4), which is related to a shift in synoptic-scale circulation patterns from predominant northerly to southerly flow over the basin (Fig. S7). The results during winter 2020–22 also highlight a correspondence between pollution levels and specific synoptic patterns (Figs. S8–S11). Furthermore, temperature inversions significantly intensified with deteriorating air quality, suggesting their potential role in exacerbating particulate pollution through suppressed vertical mixing. Such temperature inversions were related to the persistent cold-air pool phenomenon that is favorable for air pollution accumulation in Lanzhou basin (Zhang et al. 2024) and in valleys and basins in the western United States (Holmes et al. 2015).

Under the excellent level, the basin was dominated by strong northerly winds, which aligned optimally with the local topography. As pollution levels intensified, the northerly winds weakened significantly, while southerly winds gradually strengthened. Diurnal variations in slope flows were pronounced along the southern basin margin, with daytime upslope winds weakening substantially at night consistent with valley wind dynamics. Specifically, daytime valley winds reinforced northerly flow, whereas nocturnal mountain winds suppressed it. Under the good level, robust daytime upslope winds facilitated the vertical transport of pollution precursors from the basin floor to higher elevations, enhancing secondary aerosol formation (see sections 4 and 5 for more details). Under both the good and polluted

Brought to you by Lanzhou University | Unauthenticated | Downloaded 11/10/26 10:07 AM UTC

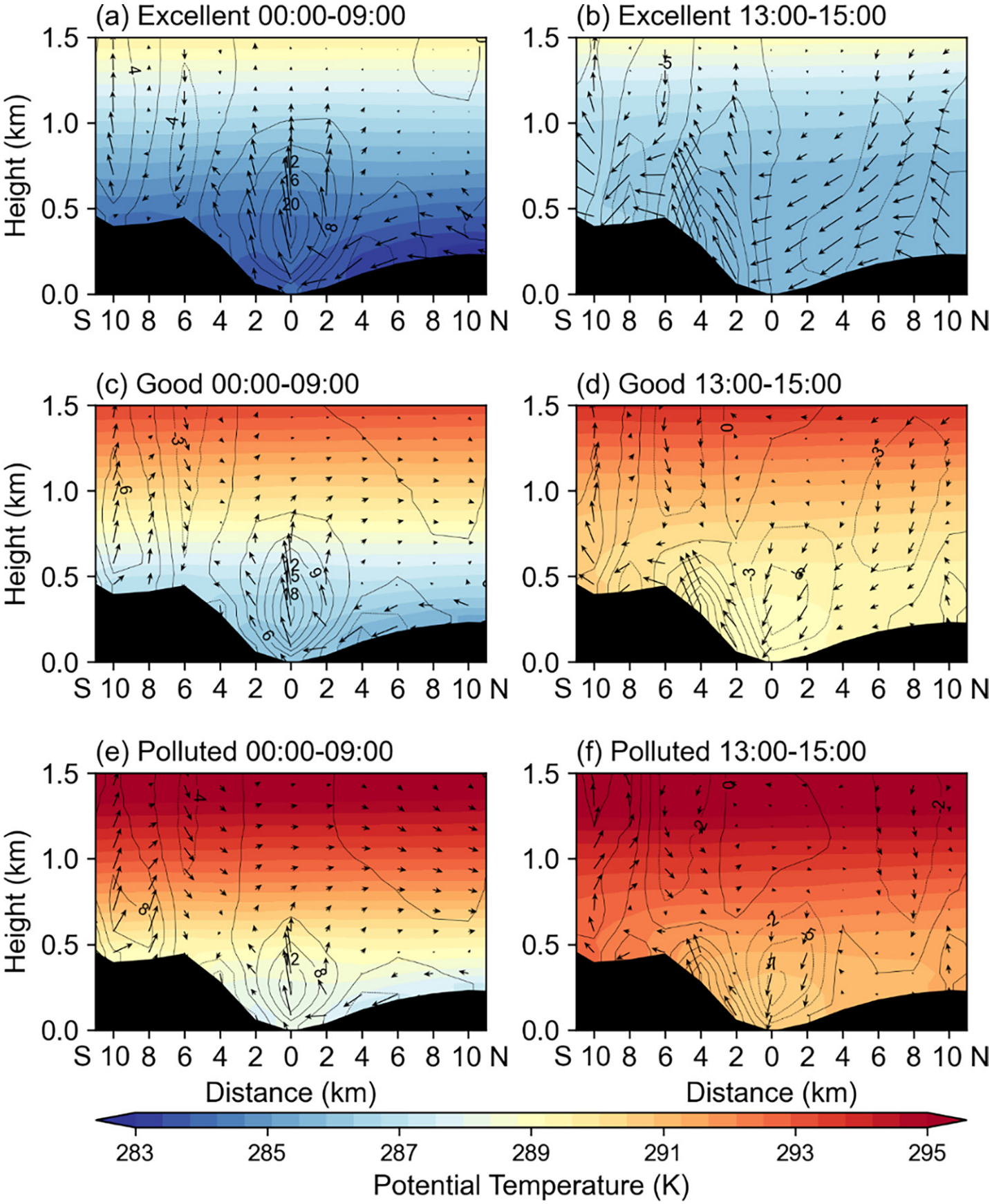


FIG. 4. **Wintertime local temperature and circulation fields in the longitudinal section across the LACMS station from WRF-Chem simulations (2020–22): (a) nighttime (0000–0900 BJT) and (b) daytime (1300–1500 BJT) under the excellent level, (c) nighttime and (d) daytime under the good level, and (e) nighttime and (f) daytime under the polluted level. The LACMS station is located at 0 km, with distances (km) to the north (N) and south (S) indicated along the horizontal axis. Black shading represents topography, colored fill denotes potential temperature (K), thin black solid lines are vertical WS contours (10^{-2} m s^{-1}), and black arrows depict the combined wind field (m s^{-1}) from vertical and meridional (north–south) components.**

Brought to you by Lanzhou University | Unauthenticated | Downloaded 11/10/26 10:07 AM UTC

levels, the interplay between southerly winds above the basin and upslope flows along the southern slope established a localized circulation, driving downward air motion toward the basin floor and thereby amplifying pollutant accumulation. Furthermore, vertical wind speeds exhibited an inverse relationship with pollution severity, indicating progressively inhibited vertical diffusion as air quality deteriorated.

Detailed boundary layer meteorological characteristics were further analyzed using intensive field observations. Measured temperature profiles reflected the evolution of synoptic weather systems and validated the WRF-Chem simulations (Fig. 5). Under the excellent level, the temperature decreased with a lapse rate close to the dry adiabatic lapse rate [γ_d = 0.98°C (100 m)$^{-1}$] from the surface to ~0.9 km, manifesting as "dry neutral," which facilitated the vertical exchange of polluted air within the basin with clean air outside the basin. In contrast, the polluted level featured a pronounced inversion layer within the basin, which can cause the decoupling of matter and energy and strongly inhibit vertical exchange. This strong inversion and associated cold-air pooling effectively decouple the boundary layer from the free troposphere, reducing vertical mixing and further concentrating pollutants near the surface. The intermediate conditions of the good level displayed thermal stratification between these extremes, with partial decoupling above ~0.3 km, allowing limited upward transport of surface-emitted precursors while still restricting exchange with the free atmosphere.

Wind direction changed from northerly to southerly within the basin from the excellent to the polluted level, further validating the WRF-Chem simulations. Mean wind speeds within the basin remained low across all conditions (2.1, 1.9, and 1.8 m s^{-1} for the excellent, good, and polluted levels, respectively), promoting pollutant accumulation. Wind speed profiles under different pollution levels intersected at ~0.35-km height, and wind speed was the lowest below the intersection and increased to the highest above the intersection until ~2.2 km under the polluted level. The vertical profiles of wind speed under the polluted level also suggested the decoupling of the boundary layer and the free troposphere (see Fig. S12 for an enlarged view of the vertical distributions of wind speed and direction below 1.5 km). Low Froude numbers (Fr < 0.3, with Fr = 0.11 under the polluted levels) confirmed limited pollutants traverse the basin top. RH was low (i.e., never exceeded 60% within the basin) and decreased with increasing severity of the pollution, which contrasts with other regions where RH increases with increasing pollution severity (Wang et al. 2016). Low RH values and the contrast RH trend suggest minimal humidity influence on winter particulate pollution in Lanzhou basin (see section 4 for more details).

The observed surface TKE exhibited a decreasing trend with increasing particulate pollution severity (Fig. 5e), underscoring the crucial role of turbulent diffusion in pollutant dispersion (Zhao et al. 2021). The profiles of Ri were further applied to diagnose turbulence in the vertical direction and thus boundary layer stability and the vertical exchange of pollutants. The Ri profiles exhibited distinct vertical variations under varying pollution levels (Fig. 5f). The Ri values generally increased from the excellent to the polluted level within the basin. Under the excellent level, Ri remained below 0.25 across the entire basin depth, with values approaching zero near the surface, indicating vigorous vertical mixing. This strong turbulent mixing facilitated efficient upward dispersion of polluted surface air masses and concurrent downward dispersion of cleaner air from upper layers, resulting in both the lowest aerosol loading and the weakest vertical decay of aerosol concentration under the excellent level (Fig. 3b). Under the good level, Ri below 0.30 km was close to Ri under the excellent level due to similar vertical trends in both shear term and buoyancy term profiles under these two pollution levels (Fig. S13), indicating that the surface polluted air masses can also be easily dispersed to the upper level of the basin. The Ri exceeded 0.25 above 0.30 km, resulting in a limited vertical exchange of air masses in and above the basin, leading to a higher aerosol loading and a faster decay in the vertical direction under the good than the excellent level.

Brought to you by Lanzhou University | Unauthenticated | Downloaded 11/10/26 10:07 AM UTC

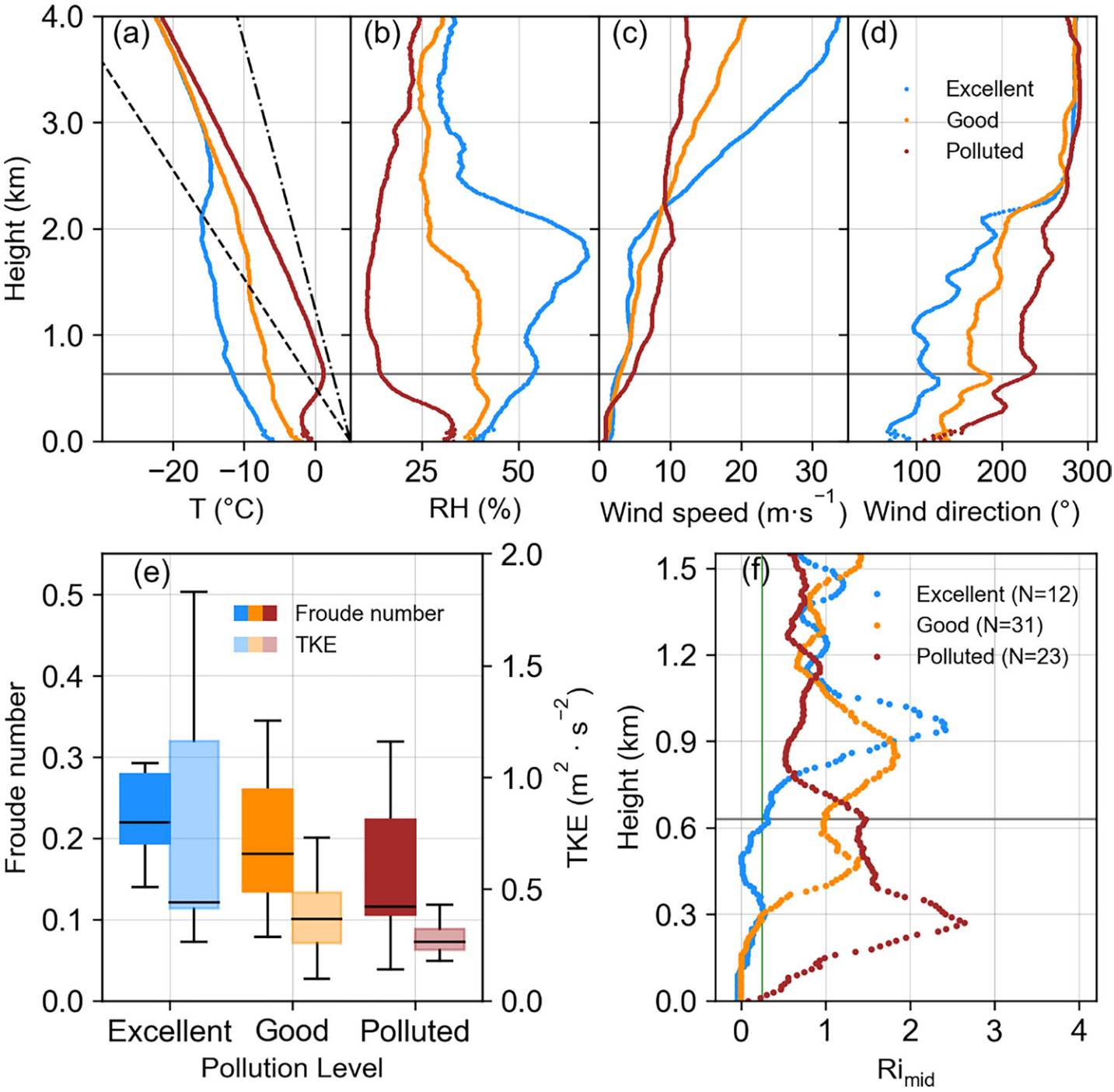


FIG. 5. Boundary layer characteristics under varying pollution levels during the January 2021 field campaign: (a) mean temperature profiles [dashed line: dry adiabatic lapse rate γ_d = 0.98°C (100 m)$^{-1}$; dotted line: moist adiabatic lapse rate γ_s = 0.4°C (100 m)$^{-1}$]; (b) mean RH profiles; (c) mean WS profiles; (d) mean WD profiles; (e) mean Froude numbers within the basin and mean TKE; and (f) median gradient Richardson number (Ri) profiles with the basin top (gray horizontal line) under the excellent, good, and polluted levels.

Under the polluted level, Ri exceeded the critical threshold of 0.25 near the surface and rapidly increased to a maximum value of 2.7 at the height of 0.27 km, indicating strongly suppressed vertical mixing. This stability severely inhibited upward transport of surface polluted air masses. While Ri gradually decreased with altitude above 0.27 km, it remained above 1.0 throughout the basin depth, indicating persistently weak downward mixing of cleaner air from above. Consequently, the combined restriction of both upward and downward air mass exchange under the polluted level resulted in substantially enhanced surface aerosol accumulation and extreme steep vertical concentration gradient.

Brought to you by Lanzhou University | Unauthenticated | Downloaded 11/10/26 10:07 AM UTC

The parameters characterizing ABL turbulence—including temperature profiles, Ri profiles, and surface TKE—exhibit significant differences across the three pollution levels. In contrast, the parameters representing local circulation—such as horizontal and vertical wind speeds within the boundary layer—remain relatively small and show limited variation among pollution levels. Therefore, ABL turbulence primarily governs the vertical distribution of aerosols rather than local circulation. Nevertheless, the observed vertical aerosol structure under different pollution levels results from the combined effects of both processes.

4. Roles of photochemistry in secondary aerosol formation under different pollution levels

Conventional understanding suggests that daytime pollutant concentrations are typically lower than nighttime levels due to more favorable dispersion conditions during daylight hours, including enhanced turbulent mixing and an elevated BLH. However, the results in this study reveal a contrasting pattern, with both $PM_{2.5}$ concentrations and aerosol extinction coefficients exhibiting higher values during daytime periods, particularly under both the excellent and good levels (Fig. 6a and Figs. S14–S17). To elucidate this distinctive diurnal pattern, the potential role of photochemical secondary aerosol formation will be subsequently analyzed below.

EC rapidly increased with increasing $PM_{2.5}$ both during daytime and nighttime (Fig. 7a), indicating the importance of primary emissions in affecting fine particulate pollution. Nocturnal EC concentrations were significantly higher than daytime levels, reflecting the unfavorable dispersion condition during nighttime (i.e., the more stable and shallower boundary layer). In contrast, secondary inorganic aerosols (SIAs) showed pronounced daytime enhancement at equivalent $PM_{2.5}$ loadings, indicating substantial secondary production during daytime.

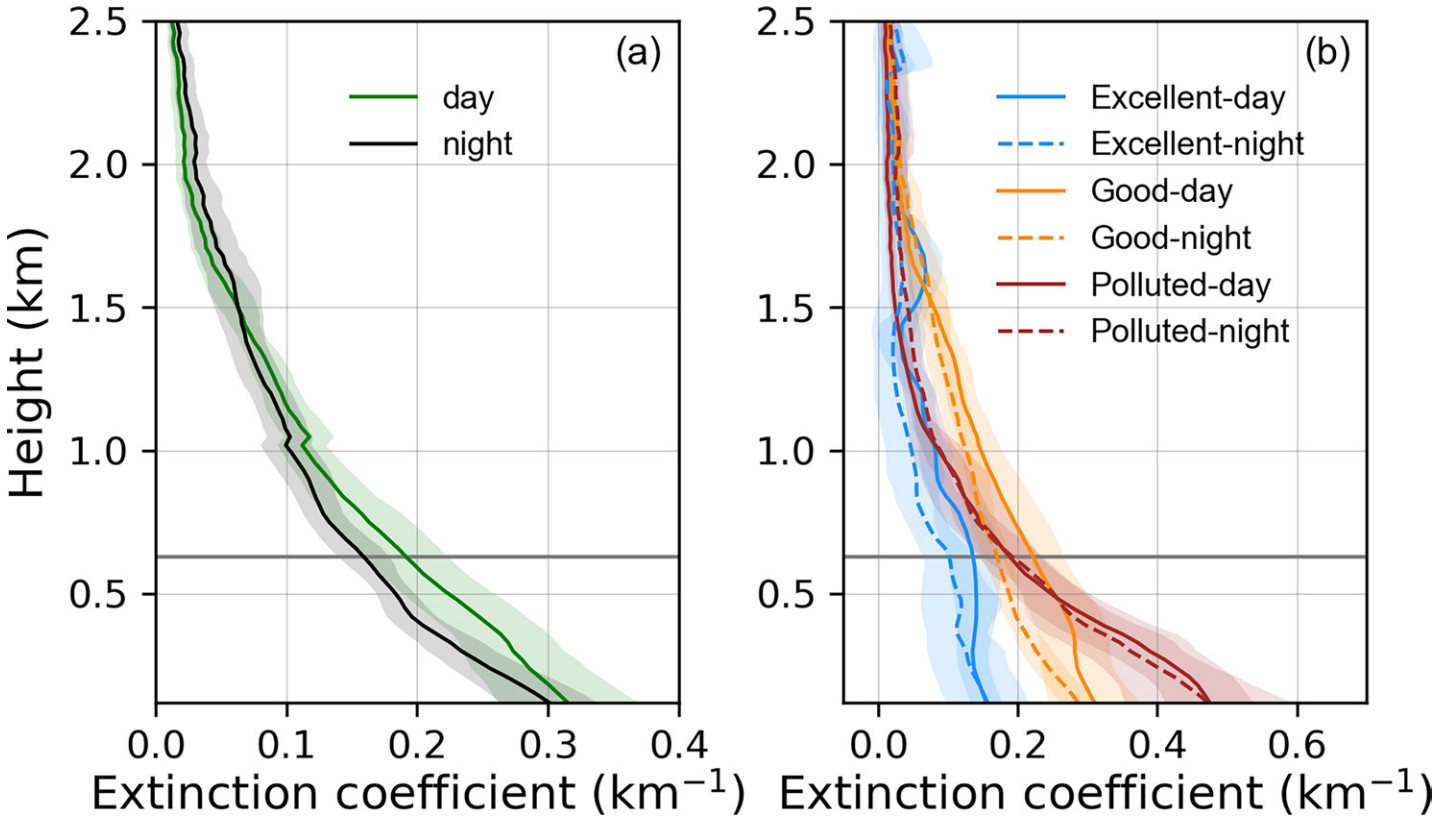


Fig. 6. Aerosol vertical distribution derived from lidar observations during the January 2021 field campaign: (a) aerosol extinction coefficients (±1 standard deviation) during daytime and nighttime and (b) aerosol extinction coefficients (±1 standard deviation) during daytime and nighttime under varying pollution levels. The gray lines represent the basin top.

Brought to you by Lanzhou University | Unauthenticated | Downloaded 11/10/26 10:07 AM UTC

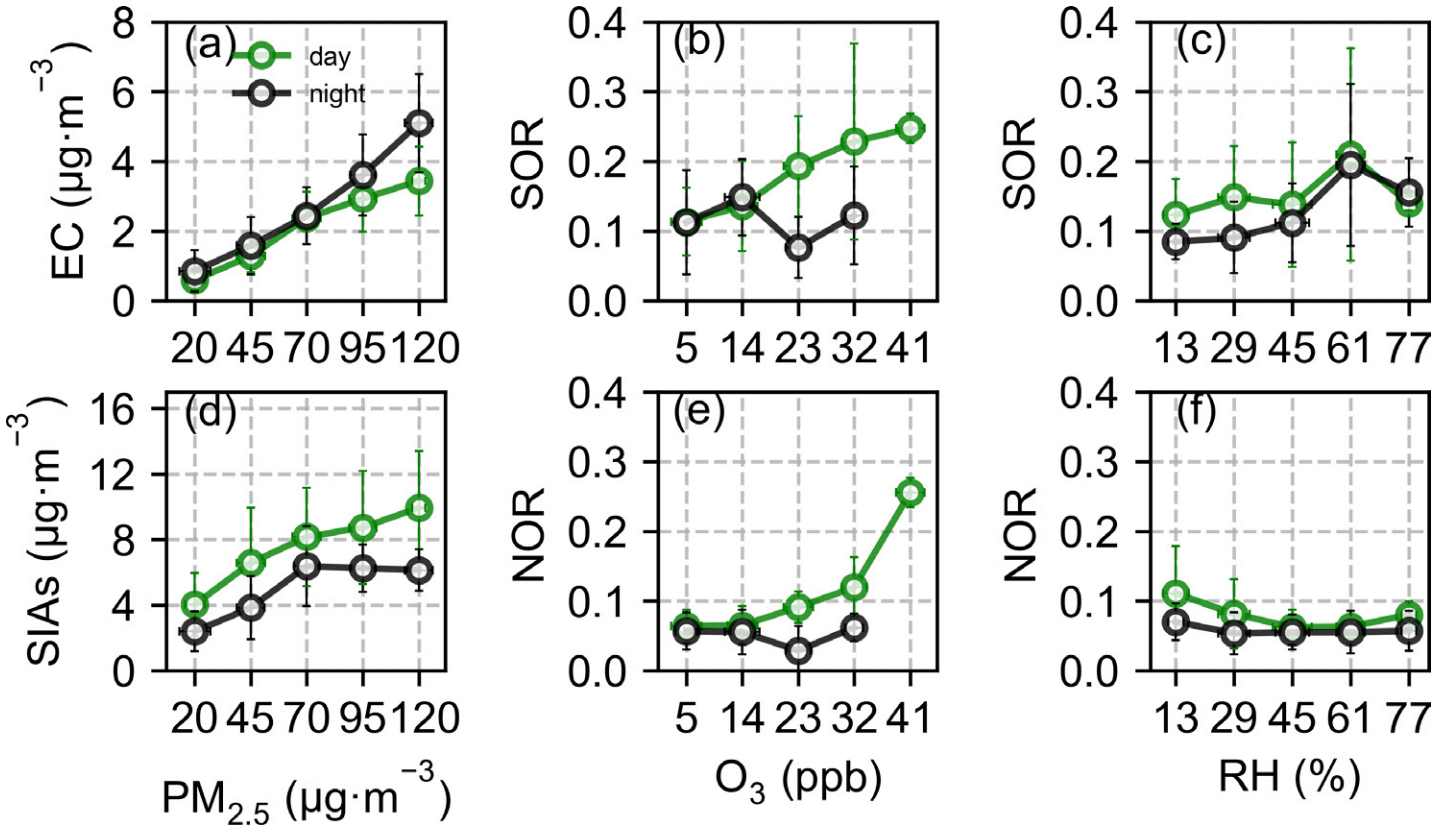


Fig. 7. Secondary aerosol formation at the LACMS station during January 2021: (a) EC and (d) SIA variation as a function of $PM_{2.5}$, SOR variation as a function of (b) ozone and (c) RH, and NOR variation as a function of (e) ozone and (f) RH.

In addition, there was little difference between daytime and nighttime secondary organic aerosols (Fig. S18).

To elucidate the dominant formation pathways of SIAs, their relationships with ozone and relative humidity were examined (Fig. 7). First, both the NOR and SOR were elevated during daytime compared to nighttime levels. Second, neither NOR nor SOR showed strong correlations with RH during either period. Most notably, while daytime NOR and SOR exhibited strong positive correlations with ozone concentrations, their nighttime counterparts showed little ozone dependence. These results collectively demonstrate that photochemical conversions, rather than heterogeneous/aqueous-phase reactions, dominate SIA formation in the Lanzhou basin. Meteorological tower-based observations in Beijing have previously revealed that the fraction of photochemical-related secondary aerosols at higher altitudes (120 and 240 m) is higher than at the surface (Lei et al. 2021). Furthermore, the steeper slope of daytime NOR versus ozone compared to SOR indicates that nitrate formation is more sensitive to photochemical processes than sulfate production.

The SIAs/EC ratio serves as a key indicator of the relative importance of secondary formation versus primary emissions in fine particulate pollution. Observation data reveal that daytime SIAs/EC ratios were significantly higher than nighttime values (Fig. S19), reinforcing the dominant role of photochemical conversion of SIAs in Lanzhou basin. Notably, under the good level, daytime SIAs/EC ratios were significantly higher than during other pollution levels, suggesting optimal photochemical conversion efficiency under this pollution level. This phenomenon aligns with vertical aerosol observations (Fig. 6b), which showed the largest diurnal differences in extinction coefficients under the good level, particularly at upper-basin levels rather than near the surface. Specifically, the largest day–night aerosol extinction coefficients difference of 0.07 km^{-1} was observed at ~0.42-km altitude under the good level.

Brought to you by Lanzhou University | Unauthenticated | Downloaded 11/10/26 10:07 AM UTC

Simultaneous measurements of aerosol chemical composition at the surface (LACMS station) and at the basin top (630 m) provided robust evidence for strong photochemistry at the upper level of the basin (Fig. 8). Surface $PM_{2.5}$ and SIA concentrations increased progressively from the excellent to the polluted level, whereas daytime concentrations at the basin top exhibited a distinct pattern—rising from the excellent to the good level but decreasing thereafter. The contrast variations in $PM_{2.5}$ and SIAs at the surface and the basin top validated the diurnal vertical extinction coefficient profiles, further demonstrating strong photochemistry at the upper level of the basin, especially under the good level.

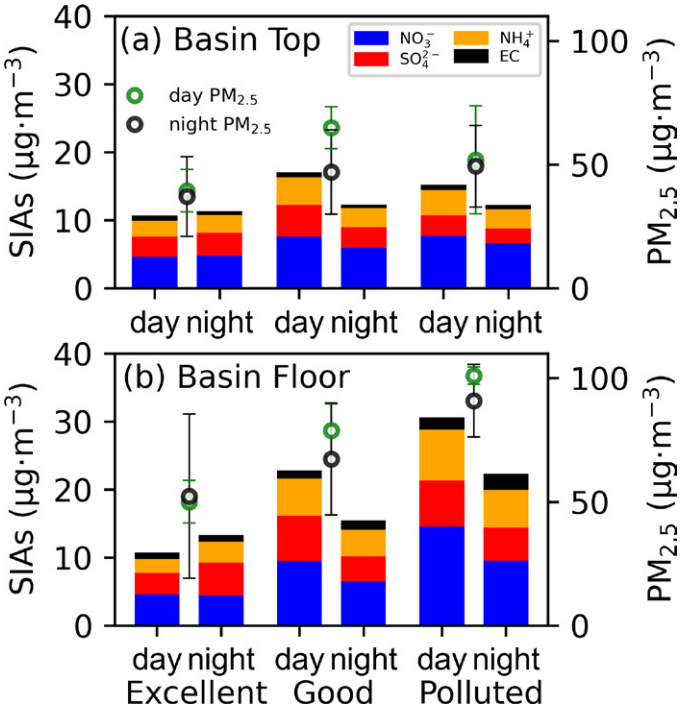


FIG. 8. $PM_{2.5}$ concentration and chemical compositions (±1 standard deviation) at the top of the basin and at the surface (LACMS station): (a) daytime and nighttime $PM_{2.5}$ and SIAs under different pollution levels at the top of the basin and (b) daytime and nighttime $PM_{2.5}$ and SIAs under different pollution levels at the LACMS station.

For clarity, we include a flowchart (Fig. 9) depicting the critical role of photochemical processes in secondary aerosol formation in the Lanzhou basin. Since our conclusion regarding the dominant role of photochemical oxidation is based on multiple observational lines of evidence, future studies employing direct observations of photochemical processes, such as aircraft- or unmanned-aerial-vehicle-based in situ measurements, will be valuable to further confirm and quantify the contribution of photochemical oxidation to secondary aerosol formation under varying boundary layer conditions. The enhanced daytime SIA production and vertical heterogeneity under the good level likely resulted from synergistic interactions between favorable photochemical activity and boundary layer meteorology under basin topography, as further discussed in section 5.

5. Discussion on the coupled effects of boundary layer meteorology and photochemistry on particulate pollution

Based on the above analysis, particulate pollution is influenced not only by boundary layer meteorology and photochemical processes individually but also significantly by their coupled effects. In Lanzhou basin, the coupled effects are characterized by the following phenomena (Fig. 10):

1) Under the excellent level, vigorous vertical exchange throughout the basin effectively transports surface pollutants upward while introducing clean air from the free atmosphere into the basin, resulting in excellent air quality.
2) Under the good level, boundary layer stability increases. While mixing remains robust in the lower layers, upper-level exchange within the basin becomes limited. This configuration allows surface-emitted precursors to reach the upper basin (~0.42 km), where enhanced ultraviolet radiation and ozone drive efficient production of SIAs, while also preventing their rapid export from the basin. Lanzhou is a relatively isolated river valley

Brought to you by Lanzhou University | Unauthenticated | Downloaded 11/10/26 10:07 AM UTC

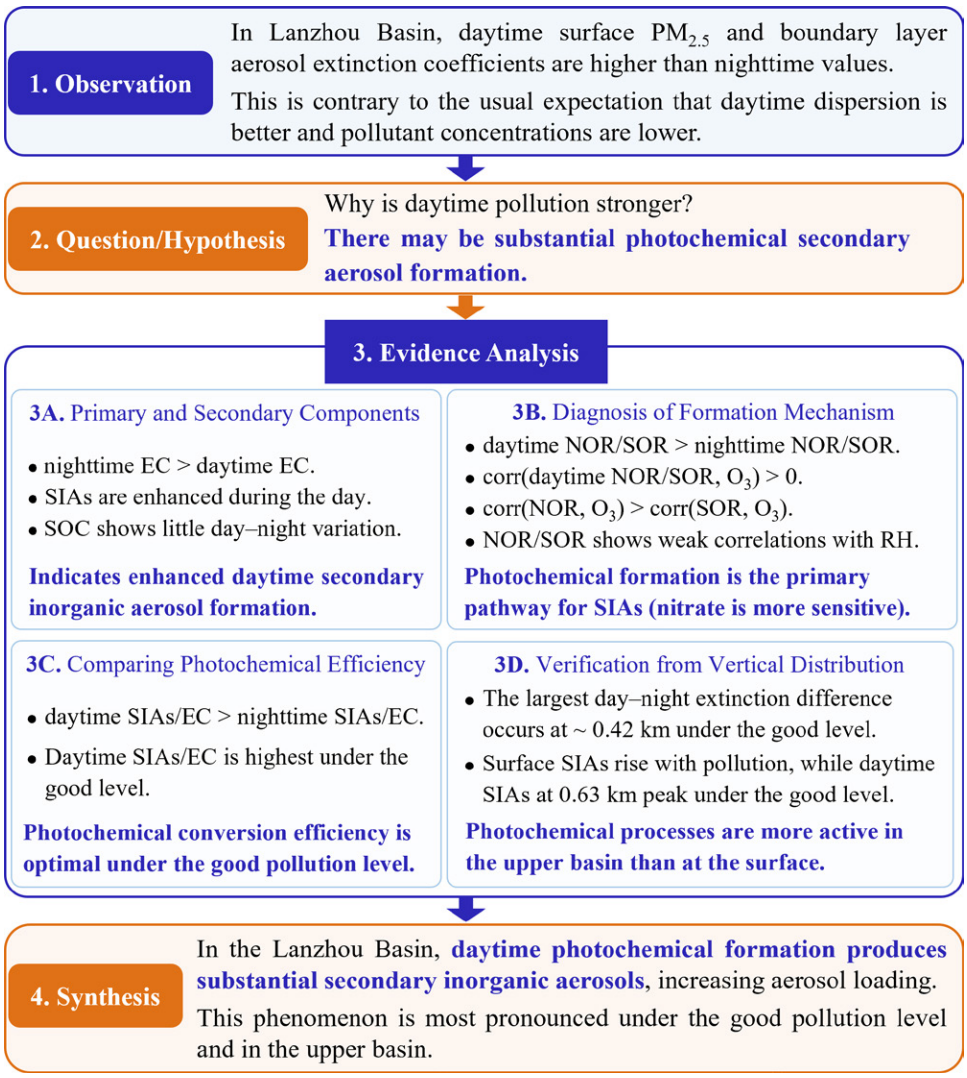


Fig. 9. Flowchart illustrating the roles of photochemistry in secondary aerosol formation in the Lanzhou basin.

basin, and most emissions originate from local anthropogenic sources. Therefore, we attribute the enhanced aerosol loading at ~0.42 km primarily to the vertical transport of precursors from the surface, which is then followed by delayed photochemical conversion in the upper ABL. Previous studies revealed that new particle formation is stronger in the upper ABL than at the surface (Lampilahti et al. 2021; Y. Wang et al. 2025), which may also contribute to the enhanced SIAs production in the upper basin in the present study.

3) The polluted level emerges when stable stratification suppresses vertical mixing throughout the boundary layer, effectively decoupling basin air from the free atmosphere. This trapping mechanism concentrates primary emissions near the surface while simultaneously reducing photochemical activity through radiation attenuation by pollutants.

We note that under certain conditions, residual layer chemistry and subsequent entrainment may also contribute to upper-level aerosol enhancements. Lidar observations during January 2021 indicated that residual layer processes were noticeably active on 5, 14, and 17 January, when pollutants accumulated above the nocturnal stable boundary layer. In these instances, entrainment of residual layer air into the convective boundary layer after sunrise promoted secondary aerosol formation aloft (supplemental Text 4). This observation is consistent with our recently published study (Li et al. 2026), which specifically quantified the

Brought to you by Lanzhou University | Unauthenticated | Downloaded 11/10/26 10:07 AM UTC

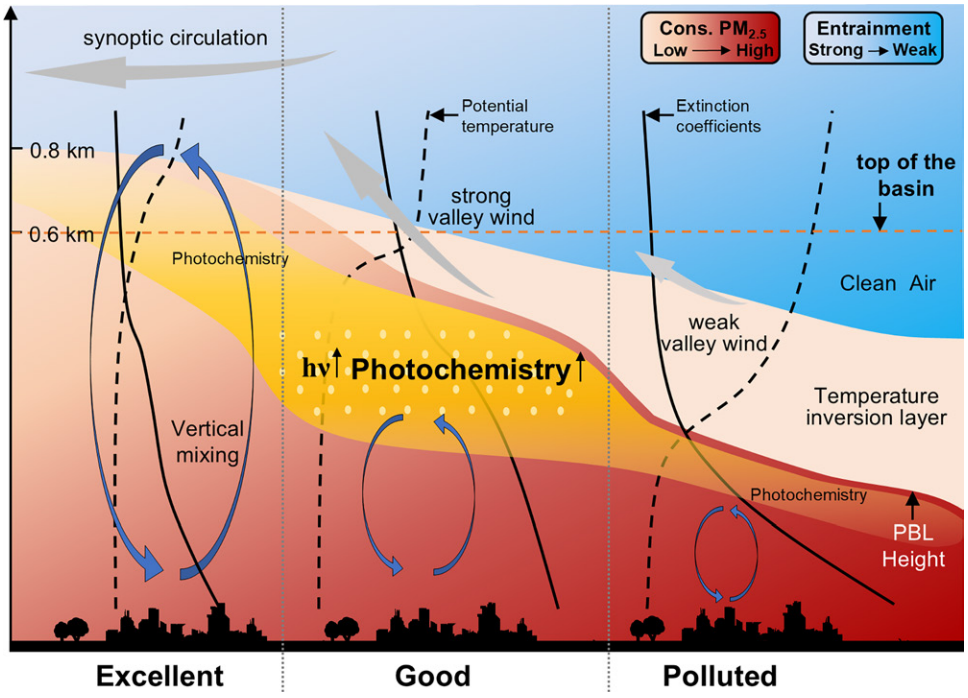


Fig. 10. Schematic diagram of boundary layer meteorology and photochemistry on aerosol vertical distribution and surface $PM_{2.5}$ pollutants in a basin city of Lanzhou with semiarid climate.

contribution of residual-layer chemistry to boundary layer nitrate in the Lanzhou basin. Using simultaneous measurements at the surface, 300, and 600 m along with large-eddy simulations, that study demonstrated that nitrate formation in the residual layer was higher than in the stable boundary layer, and its entrainment into the convective boundary layer significantly enhanced surface nitrate concentrations the following morning.

To conclude, the coupled impact of atmospheric boundary layer meteorology and photochemistry can modulate aerosol vertical mixing, affect photochemical conversion of secondary aerosols, and determine the level of particulate pollution in Lanzhou basin. The vertical mixing and photochemical SIA conversions shaped the aerosol vertical distribution and thus led to varying pollution levels. Notably, the intersection of aerosol extinction profiles under the good and the polluted levels occurs near 0.63 km, aligning closely with the basin-top height. This alignment emphasizes the role of the basin top in confining pollutants and decoupling the boundary layer from the free troposphere, which limits vertical exchange and contributes to the distinct vertical structure observed under different pollution levels. Specifically, the $PM_{2.5}$ concentrations under the polluted level were significantly higher than those under the good level despite comparable AODs under the two pollution levels. The results highlight how boundary layer meteorology–photochemistry coupling creates distinct pollution regimes that cannot be inferred from column-integrated measurements or surface observations alone. More intensive vertical observations are required to elucidate boundary layer air pollution mechanisms in addition to observational studies conducted previously (e.g., Hallar et al. 2021; Zhao et al. 2023; Y. Wang et al. 2025). Furthermore, in situ vertical observations (e.g., from aircraft and unmanned aerial vehicle platforms) are required to directly capture evidence of photochemical secondary aerosol formation and to verify the scientific mechanisms illustrated in Fig. 10.

The coupling mechanism can also be applied to other regions, particularly those with unfavorable pollutant dispersion conditions, such as the Sichuan Basin in China, basins in the western United States, and certain European basins. For example, observations at different elevations in a basin in the western United States revealed that the coupling between chemical and meteorological processes plays a dominant role in nitrate pollution under

Brought to you by Lanzhou University | Unauthenticated | Downloaded 11/10/26 10:07 AM UTC

persistent cold-air pool conditions (Baasandorj et al. 2017). A comprehensive consideration of both physical (e.g., meteorological conditions, BLH) and chemical (e.g., volatility distribution, aqueous-phase reactions) processes is essential for accurately simulating surface organic aerosol pollution in the Po Valley (Meroni et al. 2017). Through online-coupled meteorology–chemistry simulations, enhanced secondary aerosol formation has been observed in the upper boundary layer (Huang et al. 2020). Although the North China Plain is not a basin, it similarly experiences poor dispersion conditions on a regional scale (Wang et al. 2018; Zhao et al. 2020).

6. Conclusions

This study reveals the critical role of the interplay between boundary layer meteorology and photochemistry in shaping aerosol vertical distributions and surface particulate pollution based on intensive vertical observations in Lanzhou basin of northwestern China. The observations include a field campaign in January 2021 and continuous monitoring at a superstation from 2020 to 2022. The main conclusions are as follows:

1) Despite significantly different surface $PM_{2.5}$ concentrations, the columnar aerosol optical depth exhibited comparable values between the good and polluted levels due to contrasting aerosol vertical distributions. This finding highlights the important influence of aerosol vertical distribution on surface air pollution—it can even lead to differing pollution levels under similar columnar aerosol loading.
2) Peak photochemical conversion of secondary inorganic aerosols was observed in the upper ABL (~0.42-km altitude) under the good pollution level. This provides robust observational evidence for the coupled effects of ABL meteorology and photochemistry.
3) The coupling of ABL meteorology and photochemical processes modulates aerosol vertical mixing, influences photochemical formation of secondary aerosols, and ultimately determines surface particulate pollution in the Lanzhou basin. The coupling mechanism is also applicable to other regions with unfavorable pollutant dispersion conditions.

Acknowledgments. This research was supported by the Fundamental and Interdisciplinary Disciplines Breakthrough Plan of the Ministry of Education of China (JYB2025XDXM910), the National Natural Science Foundation of China (42475080 and 42205096), and the Fundamental Research Funds for the Central Universities (lzujbky-2022-it26 and lzujbky-2024-ey04). P. T., J. H., and L. Z. designed the study. P. T. and M. Z. led the writing. P. T., M. Z., X. L., Z. Y., X. S., X. G., and C. T. conducted the field campaigns and analyzed the data. All authors contributed to discussion, review, and editing.

Data availability statement. The data used in this study can be obtained by contacting the corresponding author (tianpf@lzu.edu.cn).

Brought to you by Lanzhou University | Unauthenticated | Downloaded 11/10/26 10:07 AM UTC

References

Baasandorj, M., and Coauthors, 2017: Coupling between chemical and meteorological processes under persistent cold-air pool conditions: Evolution of wintertime $PM_{2.5}$ pollution events and N_2O_5 observations in Utah's Salt Lake Valley. *Environ. Sci. Technol.*, **51**, 5941–5950, https://doi.org/10.1021/acs.est.6b06603.

Baklanov, A. A., and Coauthors, 2011: The nature, theory, and modeling of atmospheric planetary boundary layers. *Bull. Amer. Meteor. Soc.*, **92**, 123–128, https://doi.org/10.1175/2010BAMS2797.1.

Balsley, B. B., G. Svensson, and M. Tjernström, 2008: On the scale-dependence of the gradient Richardson number in the residual layer. *Bound.-Layer Meteor.*, **127**, 57–72, https://doi.org/10.1007/s10546-007-9251-0.

Canché-Cab, L., L. San-Pedro, B. Ali, M. Rivero, and M. Escalante, 2024: The atmospheric boundary layer: A review of current challenges and a new generation of machine learning techniques. *Artif. Intell. Rev.*, **57**, 331, https://doi.org/10.1007/s10462-024-10962-5.

Cao, J. J., and Coauthors, 2007: Spatial and seasonal distributions of carbonaceous aerosols over China. *J. Geophys. Res.*, **112**, D22S11, https://doi.org/10.1029/2006JD008205.

Carrillo-Cardenas, G., S. W. Hoch, E. Pardyjak, M. Garcia, W. Brown, Z. Pu, and A. G. Hallar, 2025: Elucidating new particle formation in complex terrain during the winter 2022 Cold Fog Amongst Complex Terrain (CFACT) campaign. *J. Geophys. Res. Atmos.*, **130**, e2024JD042307, https://doi.org/10.1029/2024JD042307.

Chang, Y., and Coauthors, 2022: Changes in physical and chemical properties of urban atmospheric aerosols and ozone during the COVID-19 lockdown in a semi-arid region. *Atmos. Environ.*, **287**, 119270, https://doi.org/10.1016/j.atmosenv.2022.119270.

Di Antonio, L., C. Di Biagio, G. Foret, P. Formenti, G. Siour, J.-F. Doussin, and M. Beekmann, 2023: Aerosol optical depth climatology from the high-resolution MAIAC product over Europe: Differences between major European cities and their surrounding environments. *Atmos. Chem. Phys.*, **23**, 12 455–12 475, https://doi.org/10.5194/acp-23-12455-2023.

Du, T., and Coauthors, 2020: Characteristics and formation mechanisms of winter particulate pollution in Lanzhou, northwest China. *J. Geophys. Res. Atmos.*, **125**, e2020JD033369, https://doi.org/10.1029/2020JD033369.

Fernald, F. G., 1984: Analysis of atmospheric lidar observations: Some comments. *Appl. Opt.*, **23**, 652–653, https://doi.org/10.1364/ao.23.000652.

Finardi, S., C. Silibello, A. D'Allura, and P. Radice, 2014: Analysis of pollutants exchange between the Po Valley and the surrounding European region. *Urban Climate*, **10**, 682–702, https://doi.org/10.1016/j.uclim.2014.02.002.

Geng, G., and Coauthors, 2024: Efficacy of China's clean air actions to tackle $PM_{2.5}$ pollution between 2013 and 2020. *Nat. Geosci.*, **17**, 987–994, https://doi.org/10.1038/s41561-024-01540-z.

George, C., M. Ammann, B. D'Anna, D. J. Donaldson, and S. A. Nizkorodov, 2015: Heterogeneous photochemistry in the atmosphere. *Chem. Rev.*, **115**, 4218–4258, https://doi.org/10.1021/cr500648z.

Ghude, S. D., and Coauthors, 2024: Air Quality Warning and Integrated Decision Support System for Emissions (AIRWISE): Enhancing air quality management in megacities. *Bull. Amer. Meteor. Soc.*, **105**, E2525–E2550, https://doi.org/10.1175/BAMS-D-23-0181.1.

Gu, Y., D. K. Henze, M. O. Nawaz, H. Cao, and U. J. Wagner, 2023: Sources of $PM_{2.5}$-associated health risks in Europe and corresponding emission-induced changes during 2005–2015. *GeoHealth*, **7**, e2022GH000767, https://doi.org/10.1029/2022GH000767.

Guan, X., and Coauthors, 2021: Wintertime aerosol optical properties in Lanzhou, Northwest China: Emphasis on the rapid increase of aerosol absorption under high particulate pollution. *Atmos. Environ.*, **246**, 118081, https://doi.org/10.1016/j.atmosenv.2020.118081.

Guo, J., and Coauthors, 2020: The climatology of lower tropospheric temperature inversions in China from radiosonde measurements: Roles of black carbon, local meteorology, and large-scale subsidence. *J. Climate*, **33**, 9327–9350, https://doi.org/10.1175/JCLI-D-19-0278.1.

Hallar, A. G., and Coauthors, 2021: Coupled air quality and boundary-layer meteorology in western U.S. basins during winter: Design and rationale for a comprehensive study. *Bull. Amer. Meteor. Soc.*, **102**, E2012–E2033, https://doi.org/10.1175/BAMS-D-20-0017.1.

Hao, L., and Coauthors, 2018: Combined effects of boundary layer dynamics and atmospheric chemistry on aerosol composition during new particle formation periods. *Atmos. Chem. Phys.*, **18**, 17 705–17 716, https://doi.org/10.5194/acp-18-17705-2018.

He, C., and Coauthors, 2021: Interactions between air pollution and terrestrial ecosystems: Perspectives on challenges and future directions. *Bull. Amer. Meteor. Soc.*, **102**, E525–E538, https://doi.org/10.1175/BAMS-D-20-0066.1.

Holmes, H. A., J. K. Sriramasamudram, E. R. Pardyjak, and C. D. Whiteman, 2015: Turbulent fluxes and pollutant mixing during wintertime air pollution episodes in complex terrain. *Environ. Sci. Technol.*, **49**, 13 206–13 214, https://doi.org/10.1021/acs.est.5b02616.

Huang, R.-J., and Coauthors, 2014: High secondary aerosol contribution to particulate pollution during haze events in China. *Nature*, **514**, 218–222, https://doi.org/10.1038/nature13774.

Huang, X., and Coauthors, 2020: Chemical boundary layer and its impact on air pollution in northern China. *Environ. Sci. Technol. Lett.*, **7**, 826–832, https://doi.org/10.1021/acs.estlett.0c00755.

——, Y. Wang, Y. Shang, X. Song, R. Zhang, Y. Wang, Z. Li, and Y. Yang, 2023: Contrasting the effect of aerosol properties on the planetary boundary layer height in Beijing and Nanjing. *Atmos. Environ.*, **308**, 119861, https://doi.org/10.1016/j.atmosenv.2023.119861.

Jia, W., and X. Zhang, 2020: The role of the planetary boundary layer parameterization schemes on the meteorological and aerosol pollution simulations: A review. *Atmos. Res.*, **239**, 104890, https://doi.org/10.1016/j.atmosres.2020.104890.

Kipling, Z., and Coauthors, 2016: What controls the vertical distribution of aerosol? Relationships between process sensitivity in HadGEM3–UKCA and inter-model variation from AeroCom Phase II. *Atmos. Chem. Phys.*, **16**, 2221–2241, https://doi.org/10.5194/acp-16-2221-2016.

Koelemeijer, R. B. A., C. D. Homan, and J. Matthijsen, 2006: Comparison of spatial and temporal variations of aerosol optical thickness and particulate matter over Europe. *Atmos. Environ.*, **40**, 5304–5315, https://doi.org/10.1016/j.atmosenv.2006.04.044.

Lampilahti, J., and Coauthors, 2021: Aerosol particle formation in the upper residual layer. *Atmos. Chem. Phys.*, **21**, 7901–7915, https://doi.org/10.5194/acp-21-7901-2021.

Lei, L., and Coauthors, 2021: Vertical distributions of primary and secondary aerosols in urban boundary layer: Insights into sources, chemistry, and interaction with meteorology. *Environ. Sci. Technol.*, **55**, 4542–4552, https://doi.org/10.1021/acs.est.1c00479.

Lelieveld, J., J. S. Evans, M. Fnais, D. Giannadaki, and A. Pozzer, 2015: The contribution of outdoor air pollution sources to premature mortality on a global scale. *Nature*, **525**, 367–371, https://doi.org/10.1038/nature15371.

Leung, D. M., and Coauthors, 2020: Wintertime particulate matter decrease buffered by unfavorable chemical processes despite emissions reductions in China. *Geophys. Res. Lett.*, **47**, e2020GL087721, https://doi.org/10.1029/2020GL087721.

Li, J., and Coauthors, 2026: Direct observational evidence of the influence of residual-layer vertical transport on surface nitrate concentrations in a Northern China Valley. *Atmos. Environ.*, **379**, 122085, https://doi.org/10.1016/j.atmosenv.2026.122085.

Brought to you by Lanzhou University | Unauthenticated | Downloaded 11/10/26 10:07 AM UTC

Li, Q., H. Zhang, X. Cai, Y. Song, and T. Zhu, 2021: The impacts of the atmospheric boundary layer on regional haze in North China. *npj Climate Atmos. Sci.*, **4**, 9, https://doi.org/10.1038/s41612-021-00165-y.

Li, S., E. Joseph, and Q. Min, 2016: Remote sensing of ground-level PM2.5 combining AOD and backscattering profile. *Remote Sens. Environ.*, **183**, 120–128, https://doi.org/10.1016/j.rse.2016.05.025.

Li, Y., and Coauthors, 2022: Vertically resolved aerosol chemistry in the low boundary layer of Beijing in summer. *Environ. Sci. Technol.*, **56**, 9312–9324, https://doi.org/10.1021/acs.est.2c02861.

Li, Z., and Coauthors, 2017: Aerosol and boundary-layer interactions and impact on air quality. *Natl. Sci. Rev.*, **4**, 810–833, https://doi.org/10.1093/nsr/nwx117.

Liu, S., and X.-Z. Liang, 2010: Observed diurnal cycle climatology of planetary boundary layer height. *J. Climate*, **23**, 5790–5809, https://doi.org/10.1175/2010JCLI3552.1.

Luce, H., and Coauthors, 2018: Vertical structure of the lower troposphere derived from MU radar, unmanned aerial vehicle, and balloon measurements during ShUREX 2015. *Prog. Earth Planet. Sci.*, **5**, 29, https://doi.org/10.1186/s40645-018-0187-4.

Ma, X., and F. Yu, 2014: Seasonal variability of aerosol vertical profiles over east US and west Europe: GEOS-Chem/APM simulation and comparison with CALIPSO observations. *Atmos. Res.*, **140–141**, 28–37, https://doi.org/10.1016/j.atmosres.2014.01.001.

Ma, Y., and Coauthors, 2020: The stove, dome, and umbrella effects of atmospheric aerosol on the development of the planetary boundary layer in hazy regions. *Geophys. Res. Lett.*, **47**, e2020GL087373, https://doi.org/10.1029/2020GL087373.

Meroni, A., and Coauthors, 2017: Investigating the role of chemical and physical processes on organic aerosol modelling with CAMx in the Po Valley during a winter episode. *Atmos. Environ.*, **171**, 126–142, https://doi.org/10.1016/j.atmosenv.2017.10.004.

Miao, Y., J. Li, S. Miao, H. Che, Y. Wang, X. Zhang, R. Zhu, and S. Liu, 2019: Interaction between planetary boundary layer and $PM_{2.5}$ pollution in megacities in China: A review. *Curr. Pollut. Rep.*, **5**, 261–271, https://doi.org/10.1007/s40726-019-00124-5.

Ouyang, H., and Coauthors, 2022: Toward better and healthier air quality: Implementation of WHO 2021 Global Air Quality Guidelines in Asia. *Bull. Amer. Meteor. Soc.*, **103**, E1696–E1703, https://doi.org/10.1175/BAMS-D-22-0040.1.

Pace, G., and Coauthors, 2015: On the complexity of the boundary layer structure and aerosol vertical distribution in the coastal Mediterranean regions: A case study. *Tellus*, **67B**, 27721, https://doi.org/10.3402/tellusb.v67.27721.

Platis, A., B. Altstädter, B. Wehner, N. Wildmann, A. Lampert, M. Hermann, W. Birmili, and J. Bange, 2016: An observational case study on the influence of atmospheric boundary-layer dynamics on new particle formation. *Bound.-Layer Meteor.*, **158**, 67–92, https://doi.org/10.1007/s10546-015-0084-y.

Prabhakar, G., and Coauthors, 2017: Observational assessment of the role of nocturnal residual-layer chemistry in determining daytime surface particulate nitrate concentrations. *Atmos. Chem. Phys.*, **17**, 14747–14770, https://doi.org/10.5194/acp-17-14747-2017.

Prasad, P., G. Basha, and M. V. Ratnam, 2022: Is the atmospheric boundary layer altitude or the strong thermal inversions that control the vertical extent of aerosols? *Sci. Total Environ.*, **802**, 149758, https://doi.org/10.1016/j.scitotenv.2021.149758.

Qu, W., J. Wang, X. Zhang, L. Sheng, and W. Wang, 2016: Opposite seasonality of the aerosol optical depth and the surface particulate matter concentration over the North China Plain. *Atmos. Environ.*, **127**, 90–99, https://doi.org/10.1016/j.atmosenv.2015.11.061.

Ratnam, M. V., P. Prasad, S. T. A. Raj, M. R. Raman, and G. Basha, 2021: Changing patterns in aerosol vertical distribution over South and East Asia. *Sci. Rep.*, **11**, 308, https://doi.org/10.1038/s41598-020-79361-4.

Shi, Y., and F. Hu, 2020: Ramp-like $PM_{2.5}$ accumulation process and z-less similarity in the stable boundary layer. *Geophys. Res. Lett.*, **47**, e2019GL086530, https://doi.org/10.1029/2019GL086530.

Su, T., and Coauthors, 2020: The significant impact of aerosol vertical structure on lower atmosphere stability and its critical role in aerosol–planetary boundary layer (PBL) interactions. *Atmos. Chem. Phys.*, **20**, 3713–3724, https://doi.org/10.5194/acp-20-3713-2020.

Sun, H., Y. Shi, L. Liu, W. Ding, Z. Zhang, and F. Hu, 2021: Impacts of atmospheric boundary layer vertical structure on haze pollution observed by tethered balloon and lidar. *J. Meteor. Res.*, **35**, 209–223, https://doi.org/10.1007/s13351-021-0076-4.

Thomas, A., C. Sarangi, and V. P. Kanawade, 2019: Recent increase in winter hazy days over Central India and the Arabian Sea. *Sci. Rep.*, **9**, 17406, https://doi.org/10.1038/s41598-019-53630-3.

Tian, P., and Coauthors, 2017: Aerosol vertical distribution and optical properties over China from long-term satellite and ground-based remote sensing. *Atmos. Chem. Phys.*, **17**, 2509–2523, https://doi.org/10.5194/acp-17-2509-2017.

van Donkelaar, A., R. V. Martin, and R. J. Park, 2006: Estimating ground-level $PM_{2.5}$ using aerosol optical depth determined from satellite remote sensing. *J. Geophys. Res.*, **111**, D21201, https://doi.org/10.1029/2005JD006996.

Wang, G., and Coauthors, 2016: Persistent sulfate formation from London Fog to Chinese haze. *Proc. Natl. Acad. Sci. USA*, **113**, 13630–13635, https://doi.org/10.1073/pnas.1616540113.

Wang, H., and Coauthors, 2025: Vertical gradient of nitryl chloride and implications for atmospheric photochemistry in Pearl River Delta, China, during wintertime. *Environ. Sci. Technol.*, **59**, 2144–2156, https://doi.org/10.1021/acs.est.4c08089.

Wang, L., and Coauthors, 2019: Vertical observations of the atmospheric boundary layer structure over Beijing urban area during air pollution episodes. *Atmos. Chem. Phys.*, **19**, 6949–6967, https://doi.org/10.5194/acp-19-6949-2019.

Wang, X., R. E. Dickinson, L. Su, C. Zhou, and K. Wang, 2018: $PM_{2.5}$ pollution in China and how it has been exacerbated by terrain and meteorological conditions. *Bull. Amer. Meteor. Soc.*, **99**, 105–119, https://doi.org/10.1175/BAMS-D-16-0301.1.

Wang, Y., and Coauthors, 2025: Campaign for Direct In Situ Study of Residual Layer Chemistry in Urban Beijing. *Bull. Amer. Meteor. Soc.*, **106**, E625–E641, https://doi.org/10.1175/BAMS-D-24-0127.1.

Wang, Z., L. Xue, J. Liu, K. Ding, S. Lou, A. Ding, J. Wang, and X. Huang, 2022: Roles of atmospheric aerosols in extreme meteorological events: A systematic review. *Curr. Pollut. Rep.*, **8**, 177–188, https://doi.org/10.1007/s40726-022-00216-9.

Watson-Parris, D., and Coauthors, 2019: In situ constraints on the vertical distribution of global aerosol. *Atmos. Chem. Phys.*, **19**, 11765–11790, https://doi.org/10.5194/acp-19-11765-2019.

Whiteman, C. D., S. W. Hoch, J. D. Horel, and A. Charland, 2014: Relationship between particulate air pollution and meteorological variables in Utah's Salt Lake Valley. *Atmos. Environ.*, **94**, 742–753, https://doi.org/10.1016/j.atmosenv.2014.06.012.

World Health Organization, 2021: *WHO Global Air Quality Guidelines: Particulate Matter ($PM_{2.5}$ and PM_{10}), Ozone, Nitrogen Dioxide, Sulfur Dioxide and Carbon Monoxide.* World Health Organization, 285 pp.

Xin, J., and Coauthors, 2015: The Campaign on Atmospheric Aerosol Research network of China: CARE-China. *Bull. Amer. Meteor. Soc.*, **96**, 1137–1155, https://doi.org/10.1175/BAMS-D-14-00039.1.

——, and Coauthors, 2016: The observation-based relationships between $PM_{2.5}$ and AOD over China. *J. Geophys. Res. Atmos.*, **121**, 10701–10716, https://doi.org/10.1002/2015JD024655.

——, and Coauthors, 2023: The feedback effects of aerosols from different sources on the urban boundary layer in Beijing China. *Environ. Pollut.*, **325**, 121440, https://doi.org/10.1016/j.envpol.2023.121440.

Yang, Q., and Coauthors, 2023: Antarctic atmospheric Richardson number from radiosonde measurements and AMPS. *Atmos. Chem. Phys.*, **23**, 6339–6355, https://doi.org/10.5194/acp-23-6339-2023.

Yang, X., B. Ben, W. Wang, B. Long, Y. Xie, K. Wu, and X. Zhang, 2025: Fine particulate matter pollution in the Sichuan Basin of China from 2013 to 2020:

Brought to you by Lanzhou University | Unauthenticated | Downloaded 11/10/26 10:07 AM UTC

Sources, emissions, and mortality burden. *Environ. Int.*, **197**, 109366, https://doi.org/10.1016/j.envint.2025.109366.

Yorks, J. E., and Coauthors, 2023: A SmallSat concept to resolve diurnal and vertical variations of aerosols, clouds, and boundary layer height. *Bull. Amer. Meteor. Soc.*, **104**, E815–E836, https://doi.org/10.1175/BAMS-D-21-0179.1.

Zhang, M., P. Tian, H. Zeng, L. Wang, J. Liang, X. Cao, and L. Zhang, 2021: A comparison of wintertime atmospheric boundary layer heights determined by tethered balloon soundings and lidar at the site of SACOL. *Remote Sens.*, **13**, 1781, https://doi.org/10.3390/rs13091781.

——, and Coauthors, 2024: Impact of aerosol-boundary layer interactions on $PM_{2.5}$ pollution during cold air pool events in a semi-arid urban basin. *Sci. Total Environ.*, **922**, 171225, https://doi.org/10.1016/j.scitotenv.2024.171225.

Zhang, Q., and Coauthors, 2019: Drivers of improved $PM_{2.5}$ air quality in China from 2013 to 2017. *Proc. Natl. Acad. Sci. USA*, **116**, 24 463–24 469, https://doi.org/10.1073/pnas.1907956116.

Zhang, R., and Coauthors, 2015: Formation of urban fine particulate matter. *Chem. Rev.*, **115**, 3803–3855, https://doi.org/10.1021/acs.chemrev.5b00067.

Zhang, S., and Coauthors, 2025: Exploring aerosol vertical distributions and their influencing factors: Insight from max-DOAS and machine learning. *Environ. Sci. Technol.*, **59**, 11 616–11 627, https://doi.org/10.1021/acs.est.4c14483.

Zhang, Y., and Coauthors, 2021: Aerosol physical-optical properties and PBLH under different air pollution levels from ground lidar and satellite observations over Shouxian area, China. *J. Geophys. Res. Atmos.*, **126**, e2021JD035236, https://doi.org/10.1029/2021JD035236.

Zhao, B., and Coauthors, 2018: Intra-annual variations of regional aerosol optical depth, vertical distribution, and particle types from multiple satellite and ground-based observational datasets. *Atmos. Chem. Phys.*, **18**, 11 247–11 260, https://doi.org/10.5194/acp-18-11247-2018.

Zhao, D., and Coauthors, 2020: Haze pollution under a high atmospheric oxidization capacity in summer in Beijing: Insights into formation mechanism of atmospheric physicochemical processes. *Atmos. Chem. Phys.*, **20**, 4575–4592, https://doi.org/10.5194/acp-20-4575-2020.

——, and Coauthors, 2021: The impact threshold of the aerosol radiative forcing on the boundary layer structure in the pollution region. *Atmos. Chem. Phys.*, **21**, 5739–5753, https://doi.org/10.5194/acp-21-5739-2021.

Zhao, S., J. He, L. Dong, S. Qi, D. Yin, J. Chen, and Y. Yu, 2023: Contrasting vertical circulation between severe and light air pollution inside a deep basin: Results from the collaborative experiment of 3D Boundary-Layer Meteorology and Pollution at the Sichuan Basin (BLMP-SCB). *Bull. Amer. Meteor. Soc.*, **104**, E411–E434, https://doi.org/10.1175/BAMS-D-22-0150.1.

Zheng, G. J., and Coauthors, 2015: Exploring the severe winter haze in Beijing: The impact of synoptic weather, regional transport and heterogeneous reactions. *Atmos. Chem. Phys.*, **15**, 2969–2983, https://doi.org/10.5194/acp-15-2969-2015.

Zhou, S., and Coauthors, 2020: Measurement report: Vertical distribution of atmospheric particulate matter within the urban boundary layer in Southern China—Size-segregated chemical composition and secondary formation through cloud processing and heterogeneous reactions. *Atmos. Chem. Phys.*, **20**, 6435–6453, https://doi.org/10.5194/acp-20-6435-2020.

Zhu, T., and Coauthors, 2023: Recent progress in atmospheric chemistry research in China: Establishing a theoretical framework for the "air pollution complex". *Adv. Atmos. Sci.*, **40**, 1339–1361, https://doi.org/10.1007/s00376-023-2379-0.

Brought to you by Lanzhou University | Unauthenticated | Downloaded 11/10/26 10:07 AM UTC